Robust PI Controller Design for Frequency Stabilization in a Hybrid Microgrid System considering Parameter Uncertainties and Communication Time Delay

A.Jeya Veronica[1], N. Senthil Kumar[2*], Francisco Gonzalez-Longatt[3]

[1]School of Electrical Engineering, VIT University, Chennai Campus, Chennai, India
[2]School of Electrical Engineering, VIT University, Chennai Campus, Chennai, India
[3] Centre for Renewable Energy Systems Technology—CREST, Loughborough University, Loughborough, UK
[*]senthilkumar.nataraj@vit.ac.in

Abstract: One of the major issues in the operation of an islanded microgrid (µG) is the frequency deviations caused by the variation of power production coming from non-dispatchable renewable energy sources (RES). Using an appropriate control system may allow the system to deal with the frequency deviation and allow the system frequency to be restored

to its rated value. A wide-area system frequency controller sends a control signal to each of the dispatchable generating sources to enforce the frequency control by using communication channels. However, the communication channels are susceptible to the time-delays which affect the performance of the frequency control system and potentially the system security. Also, the system parameters are uncertain due to the error in modelling, variation in network topology, generations, loads etc. This paper proposes a robust PI (proportional and integral) system frequency controller based on Kharitonov Theorem (KT) considering the time-delay of the communication system and the system parametric uncertainties. Simulation results demonstrate that the KT-based controller model has enhanced robustness compared to the conventional approaches of controller design.

1. Introduction

A μG consists of renewable energy resources (RESs) like wind and PV. Along with RESs, other energy resources like DG, FC and BESS are present. The mismatch between the μG power generation and the load leads to frequency instability [1]. The frequency stabilization in μG is difficult due to the low inertia of micro sources connected [2] and intermittent nature of wind and PV. To minimize the frequency deviation, coordinated control and integration of all energy sources has been done [3]. To maintain the μG frequency within the permissible limits, a suitable control strategy has to be adopted. The following paragraphs present a brief review of state of the art on the control strategies adopted for frequency regulation in μGs.

An islanded μG involving RESs, like wind power generation (WPG) and photovoltaic (PV) systems, experiences very complex frequency deviations because of the intermittent/highly-variable nature of the primary energy source (wind and sunlight, respectively) [4]. To avoid such frequency variations, it is a typical practice storing of energy from WPG and PV during peak generation to charge battery energy storage system (BESS). The BESS has an advantage of providing active power almost instantly. Moreover, it acts as a spinning reserve and an uninterruptible power supply (UPS). Because of these reimbursements, BESS is employed in the μG for the effective frequency control. As a μG comprises of WTG, PV, fuel cell (FC), diesel generator (DG), micro-turbine (MT) etc., BESS is capable of absorbing/delivering the power when wind power is more/less. Since, MT, DG, FC and PV respond gradually to meet the load, BESS delivers the active power instantly and participates in the frequency

control [2].

The system frequency gets reduced from the nominal value due to a deficit in power generation concerning the system load. During extreme power imbalance conditions, it is a common practice to shed some part of the load to reinstate the frequency to the nominal value [1]. Also, the frequency is maintained within limits by the combination of smart load and BESS by absorbing/delivering the active power to the μG which is supplied by the power of micro-hydro and wind power plants [5]. Likewise, superconducting magnetic energy storage system (SMES) and BESS provide primary frequency control (PFC) in a μG to reduce the frequency deviations which is caused by the renewable sources like WTG and PV [6]. Similar to BESS, FC can be used to improve frequency regulation. In this regard, a control strategy is developed in which FC acts as longtime energy storage, whereas flywheel (FW) acts as short time energy storage. During high wind speeds, FW stores the kinetic energy, whereas aqua electrolyser (AE) absorbs the wind power to produce hydrogen gas to feed FC. During low wind speeds, FW and FC release energy to meet the demand [7].

Apart from the coordination of FC with FW, FC combines with double layer ultra-capacitor to reduce the frequency deviations when power generated from WTG and PV systems are not adequate because of their discontinuous nature [8]. Even DG source can also be used to control the frequency deviations. The power from WTG and PV vary with time resulting in system frequency deviations [2]. When power from these generating sources are inadequate, DG controlled by the conventional automatic generation control contributes additional power to restore the system frequency within few seconds with fewer overshoots [9]. A multi-agent-based control concept is developed for a μG, where a central controller tracks the present status of the loads and the power generation from the sources. On the basis of these statuses, the central controller generates a signal such that whenever power from wind and solar are adequate to meet the loads, DG and FC should not generate any power. Meanwhile, DG and FC should generate excess power when power output from wind and solar is less to control the frequency deviations [10].

A type 2- fuzzy PI controller is adopted for the electric vehicle (EV) for the effective frequency control of the μG [11]. For the effective frequency control, the WTGs and the BESS are integrated and works well by adopting droop characteristics for WTGs [12]. In load frequency control (LFC) of μG, when the frequency change is detected, the controller transmits a signal to the generating sources to increase or decrease the power output using a communication channel. The communication channels are liable for time-delays [13]. While designing the controller, the impact of time delay should be considered. The frequency stabilization in the μG with the presence of time delay is achieved by using a T-S fuzzy model. [14].

To find the maximum permissible communication time

delay in a μG, a small model based method is used [15]. For the μG comprising of WTG, PV, DG, FC, FESS and BESS, the PI controller is adopted for the DG and FC system. IMC method is employed to find the PI parameters considering the time delay [16].

A non-linear sliding mode control (SMC) is adopted for the time delayed μG comprising of EV, PV, WTG, DG, BESS and FESS [17]. Time delay approaches have been done for the μG consisting of PV and DG. Time delay margin has been found by Rekasius substitution and decomposition like sum of squares [18].

Moreover, the frequency controller design should be accountable for the uncertainties due to an error in modelling, variations in loads and other dynamics. Because of the uncertainties, the parameters of the system are not fixed. While designing the load frequency controller, system parametric uncertainties have to be considered [19]. Usually, the parameters of distributed generation units are not constant. The parameters are uncertain due to errors in modeling and other factors. To overcome parameter uncertainty, a robust finite time control structure is adopted [20].

H-infinity method is adopted to find the PI controller parameters considering the parameter uncertainties for the MT and aqua electrolyzer (AE) [21]. PI controller is designed and adopted for wind diesel system with uncertainties of the μG to restore the frequency deviation [22]. An improvement method is applied to the multi distributed energy resources with the parameter uncertainties to improve the frequency stabilization [23].

KT provides the solution for the parametric uncertainties in which the parameters are varied between a lower bound to the upper bound. KT is implemented and tested with parameter uncertainties in load frequency control design for a conventional power system comprising of thermal plants without time-delay [24]. The literature reviews discussed above have considered either the communication time-delays or the parameter uncertainties while designing the load frequency controller for the μG. Hence, the main objective of this paper is to propose a robust PI controller based on KT which takes into an account of the parameter uncertainties and communication time-delay inherent in the μG.

This paper is organised as follows: Section 2 explains the main sources and the effects of communication time-delay existing in the μG. Section 3 explains the generalised KT. Section 4 explains the dynamic modelling of the μG. Section 5 explains the computation of PI parameters for time-delay system. Section 6 explains the application of KT for DG and FC systems with and without time-delay. Section 7 presents the results of an illustrative numerical example where the proposed methodology is applied. Section 8 and 9 present the simulation results and conclusion.

2. Communication Time-delay in Frequency Control Systems

The μG has three levels of hierarchical control structure: Distribution network operator (DNO), μG central controller (μGCC) and local controllers (LCs). The μGCC is responsible for the reliable operation of the distributed energy resources (DERs) in meeting the load. The DNO makes the μG interact with the distribution network. The LCs control the DERs within the μG. In a decentralised control, LC communicates with the μGCC and also with other LCs with the intention of exchanging some information applicable to the operation of the μG. The decentralised control needs for information about the frequencies and voltages measured by the other DERs [25]. Once the frequency change is detected, the controller transmits a control signal to the generating sources to increase or decrease the power output using a communication channel. The communication channels are liable for time-delays [13]. The time-delays in the communication channels can negatively affect the control system performance [26]. For instance, large time-delays cause instability of the systems, i.e. the frequency deviation will diverge extremely from the nominal value [27]. Several methods are available to calculate the maximum value of time-delay that promises the stability of the system in the literature. In [28], based on the frequency domain approach, a direct method is proposed. In [29], based on the gain and phase margin of the system, maximum time-delay is found. In [30], an indirect method based on linear matrix inequality (LMI) and Lyapunov theory are discussed. The focus of this paper is to find the stable PI controller values by applying KT for time-delay systems which are not applied in LFC of μG yet.

3. Generalised Kharitonov Theorem

Routh-Hurwitz criterion can be used for the assessment of the stability of a dynamic system with fixed parameters. In real life, no practical system can be derived into its exact dynamic model because of the uncertainties existing in the system. For a system having significant parameter uncertainties, KT provides the solution for synthesising the controller parameters such that the coefficients of the characteristic polynomial are within a range (since the parameters are uncertain) [20] and referred to as interval plants.

Consider an interval polynomial, $p(s,C)$, defined as [20]:

$$P \triangleq \{p(s,C) = c_0 + c_1 s + \cdots c_n s^n : c_i \subset C, c \in [c_i^-, c_i^+]\} \tag{1}$$

where $c_i^-, c_i^+ \in \mathbb{R}$ with $c_i^- \leq c_i^+, \forall_i = 0,1,2,\ldots,n$, and $c_i^-, c_i^+ \neq 0$ and $c_i = [c_i^-, c_i^+]$, c_i^- and c_i^+ represents the lower and upper bound of the interval parameters.

The four related Kharitonov polynomials defined for the interval polynomial p, (1) are:

$$Q_1(s) = c_0^- + c_1^- s + c_2^+ s^2 + c_3^+ s^3 + \cdots \tag{2}$$

$$Q_2(s) = c_0^- + c_1^+ s + c_2^+ s^2 + c_3^- s^3 + \cdots \tag{3}$$

$$Q_3(s) = c_0^+ + c_1^- s + c_2^- s^2 + c_3^+ s^3 + \cdots \tag{4}$$

$$Q_4(s) = c_0^+ + c_1^+ s + c_2^- s^2 + c_3^- s^3 + \tag{5}$$

3

The above presented four polynomials $\{Q_1, Q_2, Q_3, Q_4\}$ make a set of eight subsystems if the system model is in the form of a transfer function $G(s)$: $G(s) = \frac{(b_i^-, b_i^+)}{P(s,C)}$ where $b_i^-, b_i^+ \in \mathbb{R}$ as

$$G_1(s) = \frac{b_i^-}{Q_1(s)}, G_2(s) = \frac{b_i^+}{Q_1(s)}, G_3(s) = \frac{b_i^-}{Q_2(s)},$$
$$G_4(s) = \frac{b_i^+}{Q_2(s)}, G_5(s) = \frac{b_i^-}{Q_3(s)}, G_6(s) = \frac{b_i^+}{Q_3(s)}, \quad (6)$$
$$G_7(s) = \frac{b_i^+}{Q_4(s)}, G_8(s) = \frac{b_i^-}{Q_4(s)}$$

where b_i^+ and b_i^- are the upper bound and lower bound of the numerator polynomial.

3.1. Computation of PI Parameters

Consider an interval system defined by the transfer function, $G(s)$:

$$G(s) = \frac{N(s)}{M(s)} \quad (7)$$

and the transfer function of PI controller, $G_c(s)$ is defined as:

$$G_c(s) = (K_p s + K_i)/s \quad (8)$$

where K_p is proportional gain and K_i is integral gain of the PI controller. Substitute $s = j\omega$ and split $N(s)$ and $D(s)$ of (7) into their real and imaginary parts we obtain

$$G(j\omega) = \frac{N_{real} + j\omega N_{imag}}{M_{real} + j\omega M_{imag}} \quad (9)$$

where N_{imag}, N_{real}, M_{imag} and M_{real} are real and imaginary parts of numerator and denominator respectively. The closed-loop characteristic equation, $\Delta(s)$ can be written as:

$$\Delta(s) = 1 + G_c(s)G(s) \quad (10)$$

Substitute (8) and (9) in (10), then the closed-loop characteristic equation is transformed into:

$$\Delta(j\omega) = [K_i N_{real} - \omega^2 K_p N_{imag} - \omega^2 M_{imag}] + j\omega[\omega(K_i N_{imag} + K_p N_{real} + M_{real})] \quad (11)$$

The real part of (11) can be written as

$$\text{Re}[\Delta(j\omega)] = [K_i N_{real} - \omega^2 K_p N_{imag} - \omega^2 M_{imag}] \quad (12)$$

The imaginary part of (11) can be written as

$$\text{Im}[\Delta(j\omega)] = [(K_i N_{imag} + K_p N_{real} + M_{real})] \quad (13)$$

The integral gain of the controller is obtained by equating (12) to zero

$$K_i = \frac{\omega^2 K_p N_{imag} + \omega^2 M_{imag}}{N_{real}} \quad (14)$$

Substitute (14) in (13), finally the proportional gain of the controller is calculated as:

$$K_p = \frac{-(N_{real} M_{real} + \omega^2 N_{imag} M_{imag})}{(N_{real}^2 + \omega^2 N_{real}^2)} \quad (15)$$

The proportional gain is obtained by equating (13) to zero

$$K_p = \left[\frac{(-K_i N_{imag} - M_{real})}{N_{real}}\right] \quad (16)$$

Substitute (16) in (12), finally the integral gain of the controller is calculated as:

$$K_i = \frac{\omega^2(N_{real} M_{imag} - M_{real} N_{imag})}{(N_{real}^2 + \omega^2 N_{imag}^2)} \quad (17)$$

The equations (15) and (17) allow the calculation and plotting of the stability boundary locus (SBL) $\varphi(K_p, K_i, \omega)$ as a function of the values of ω. Describe the set $J(G(s)G_c(s))$ which contains all stable values of PI controller $G_c(s)$ which stabilizes $G(s)$. Then, the set of all stabilizing values of PI controller can be written as $J(G(s)G_c(s)) = J(G_1(s)G_c(s)) \cap J(G_2(s)G_c(s)) \dots J(G_8(s)G_c(s))$ (using (6)). The stable values of the PI controller parameters, K_p(proportional gain) and K_i (integral gain), are taken from the region where maximum loci are intersected [33].

4. μG Configuration and System Modelling

This section presents the configuration of the hybrid μG considered in this paper, and the main details of the linearized model used to describe its frequency regulation. The arrangement of the hybrid μG system comprising of WTG, DG, FC, and BESS is shown in Fig. 1.
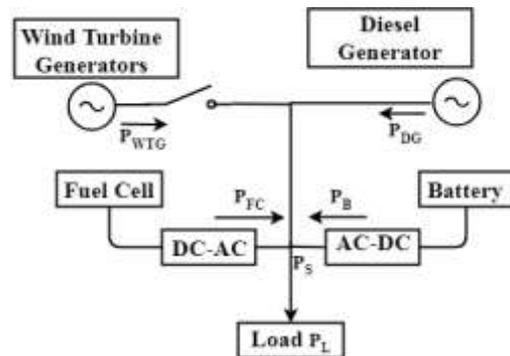
*Fig. 1. Schematic diagram of the Hybrid μG System.*

The total power, P_s supplied to the load in the lossless system is given by

$$P_s = P_{WTG} + P_{DG} + P_{FC} \pm P_{BESS} \quad (18)$$

where P_{WTG}, P_{DG}, P_{FC}, and P_{BESS} are the active power outputs of the WTG, DG, FC and BESS, respectively.

4.1 Wind Turbine Generator

The wind speed is the main variable that determines the output power of the WTG. The mechanical power output of a wind turbine depends on the power coefficient (C_p) which is the ratio of the tip speed ratio and blade pitch angle (β). The tip speed ratio (λ) is the ratio between the tangential speed of the tip of a blade to the wind speed (V_w) and can be expressed as

$$\lambda = R * \omega / V_w \qquad (19)$$

where R is the radius of the wind turbine rotor, ω is the blade angular speed, and Vw is the wind speed. The wind turbine mechanical power output (P_W) is expressed as

$$P_W = 0.5 \, \rho \, A_r C_p V_w^3 \qquad (20)$$

where ρ is the air density, and A_r is the area swept by the wind turbine rotor [31]. With the gain and time constants (K_{WTG} and T_{WTG}), the transfer function (G_{WTG}) representing the changes in frequency dynamic of the WTG [31] is:

$$G_{WTG}(s) = \frac{K_{WTG}}{1 + sT_{WTG}} \qquad (21)$$

4.2 Diesel Generator

DG is a dispatchable power source; as a consequence, the output power can be used to compensate changes its output power with the varying wind power in a shorter period. The transfer function (G_{DG}) representing the frequency dynamic of the DG, including the droop regulation R [34], is:

$$G_{DG}(s) = \frac{1}{1 + sT_G} * \frac{1}{1 + sT_T} \qquad (22)$$

where T_G and T_T are the time constants of the speed governing system and the diesel power generation system, respectively.

4.3 Fuel Cell Generator

FC consists of anode, cathode and an electrolyte. As the hydrogen gas (H_2) passed to the anode, it is divided into hydrogen ions (H^+) and electrons (e^-). These electrons pass through the anode to the external circuit and the cathode. Meanwhile, oxygen (O_2) is sent to the cathode and hydrogen ions (H^+) pass through the electrolyte and reach the cathode where they are converted to water (H_2O). The FC power output is connected to the μG through an inverter and the interconnection device. The transfer function describing the frequency dynamic of the FC (G_{FC}), inverter and interconnection device [34] is given as:

$$G_{FC}(s) = \frac{1}{1 + sT_{FC}} * \frac{1}{1 + sT_{IN}} * \frac{1}{1 + sT_{IC}} \qquad (23)$$

where T_{FC}, T_{IN}, and T_{IC} are the time constants of the FC, inverter and interconnection respectively.

4.4 Battery Energy Storage System

The BESS is capable of quickly delivering active power following load changes. When the power deficit occurs, BESS discharges power into the network and charges when power generation is high. With the gain and time constants (K_{BESS} and T_{BESS}), the BESS transfer function defining the frequency dynamic [31] (G_{BESS}) is:

$$G_{BESS}(s) = \frac{K_{BESS}}{1 + sT_{BESS}} \qquad (24)$$

4.5 Power and Frequency Deviations

The power difference (ΔP_e) between the power generation P_s and the load demand P_s^* is given by

$$\Delta P_e = P_s - P_s^* \qquad (25)$$

The system frequency Δf is represented as the ratio between the power difference (ΔP_e) and the system frequency characteristic constant (K_{sys})

$$\Delta f = \Delta P_e / K_{sys} \qquad (26)$$

with the inertia (M) and damping (D) constant, the transfer function of the μG (G_{sys}) is expressed as [31]

$$G_{sys}(s) = \Delta f / \Delta P_e = 1/K_{sys}\big(1 + sT_{sys}\big) = 1/Ms + D \qquad (27)$$

The dynamic model of LFC of hybrid μG system with time-delay is shown in Fig. 2. The communication delay is given in the exponential form as e^{-Ls}. L denotes the time-delay. K_1 and K_2 are called frequency bias factors which are obtained using Zieglers-Nichols tuning method [32]. The rated power, gain and time constants [34] of the sources are given in Table I, and Table II.

5. Computation of PI Parameters for Time-delayed Systems

Consider a plant with time-delay [35]; it is represented by the following transfer function, $G(s)$:

$$G(s) = \frac{N(s)}{M(s)} e^{-Ls} \qquad (28)$$

and the transfer function of the PI controller $G_c(s)$ is given as:

$$G_c(s) = (K_p s + K_i)/s \qquad (29)$$

Substituting $s = j\omega$ and splitting $N(s)$ and $M(s)$ of (28) into their real and imaginary parts, the plant transfer function is rewritten as:

5

$$G(j\omega) = \frac{N_{real} + j\omega N_{imag}}{M_{real} + j\omega M_{imag}} \quad (30)$$

Take (10), substitute (29) and (30) and separating into real and imaginary parts, the closed-loop characteristic equation $\Delta(s)$ is:

$$\Delta(s) = \left[(K_i N_{real} - K_p \omega^2 N_{imag})cos(\omega L) + \omega(K_i N_{imag} + K_p N_{real})sin(\omega L) - \omega^2 M_{imag}\right] + j\left[\omega(K_i N_{imag} + N_{real})cos(\omega L) - (K_i N_{real} - \omega^2 K_p N_{imag})sin(\omega L) + \omega M_{real}\right] \quad (31)$$

Equating the real and imaginary parts of (31), we obtain

$$K_p\left[-\omega^2 N_{imag}cos(\omega L) + \omega N_{real}sin(\omega L)\right] + K_i\left[N_{real}cos(\omega L) - \omega N_{imag}sin(\omega L)\right] = \omega^2 M_{imag} \quad (32)$$

and

$$K_p\left[\omega N_{real}cos(\omega L) + \omega^2 N_{imag}sin(\omega L)\right] + K_i\left[\omega N_{imag}cos(\omega L) - N_{real}sin(\omega L)\right] = -\omega M_{real} \quad (33)$$

The equation (32) and (33) can be rewritten in terms of the following components:

$$A(\omega) = \omega N_{real}sin(\omega L) - \omega^2 N_{imag}cos(\omega L),$$
$$B(\omega) = N_{real}cos(\omega L) + \omega N_{imag}sin(\omega L),$$
$$X(\omega) = \omega^2 M_{imag}$$
$$(34)$$

$$H(\omega) = \omega N_{real}cos(\omega L) + \omega^2 N_{imag}sin(\omega L),$$
$$I(\omega) = \omega N_{imag}cos(\omega L) + N_{real}sin(\omega L),$$
$$Y(\omega) = -\omega M_{real}$$
$$(35)$$

Substituting (34) and (35) in (32) and (33), then;

Table II. Parameters of the dynamic models used in the hybrid μG system [34].

Parameter	Value	Parameter	Value
D	0.0150	T_{FC}	0.2600
M	0.1667	T_{IC}	0.0040
T_G	0.0800	T_{IN}	0.0400
T_T	0.4000	R	3.0000
K_1	10.0000	K_2	10.0000
T_{BESS}	0.1000	K_{WTG}	1.0000
K_{BESS}	1.0000	T_{WTG}	1.5000

$$K_p A(\omega) + K_i B(\omega) = X(\omega) \quad (36)$$

$$K_p H(\omega) + K_i I(\omega) = Y(\omega) \quad (37)$$

Multiplying (36) by $I(\omega)$, (37) by $B(\omega)$ and solving, the proportional gain is obtained as a function of *A, B, H, I, X* and *Y*:

$$K_p = \frac{X(\omega)I(\omega) - Y(\omega)B(\omega)}{A(\omega)I(\omega) - B(\omega)H(\omega)} \quad (38)$$

Multiplying (36) by $H(\omega)$ and (37) by $A(\omega)$; the proportional gain is obtained as a function of *A, B, H, I ,X* and *Y*:

$$K_i = \frac{Y(\omega)A(\omega) - X(\omega)H(\omega)}{A(\omega)I(\omega) - B(\omega)H(\omega)} \quad (39)$$

Substituting (34) and (35) into (38) and (39), the explicit equation of the proportional gain is obtained as:

$$K_p = \frac{\gamma_1 cos(\omega L) + \omega \gamma_2 sin(\omega L)}{-(N_{real}^2 + \omega^2 N_{imag}^2)} \quad (40)$$

Finally, the explicit equation of the integral gain is obtained as:

$$K_i = \frac{\omega^2 \gamma_3 cos(\omega L) - \omega \gamma_4 sin(\omega L)}{-(N_{real}^2 + \omega^2 N_{imag}^2)} \quad (41)$$

where $\gamma_1 = \omega^2 N_{imag}M_{imag} + N_{real}M_{real}$, $\gamma_2 = N_{imag}M_{real} - N_{real}M_{imag}$, $\gamma_3 = N_{imag}M_{real} - N_{real}M_{imag}$, $\gamma_4 = N_{real}M_{real} - \omega^2 N_{imag}M_{imag}$

Thus, for any system with the time-delay (L), the PI controller parameters can be found using (40) and (41). This section explained the finding of PI for fixed system parameters. As the system parameters are in the interval form, the following Section 6 explains the implementation of KT for time-delay systems.

6 Application of KT for DG and FC Systems With and Without Time-delay

6.1 KT for Finding PI parameters for DG with time-delay

The transfer function of the diesel generator considering time delay in (42) is obtained by multiplying equation (22) with $e^{-Ls} * \frac{k_p}{1+sT_p}$.(In (42), K_p and T_p can be calculated from, $(1/Ms+D)=((1/D)/(M/Ds+1))=(K_p/T_p s+1))$.

$$G_{DG}(s) = \frac{K_p * e^{-Ls}}{\alpha_1 s^3 + \alpha_2 s^2 + \alpha_3 s + \alpha_4} \quad (42)$$

where $\alpha_1 = T_G T_T T_P$, $\alpha_2 = T_G T_T + T_T T_P + T_G T_P$, $\alpha_3 = T_G + T_T + T_P$, $\alpha_4 = 1 + \frac{K_P}{R}$

For the DG dynamic model with droop characteristics (42), the closed droop characteristics (10) with PI controller of the

6

form (8) are given by the closed-loop characteristic equation $\Delta(s)$:

$$\Delta(s) = 1 + \left(K_p + \frac{K_i}{s}\right)\frac{K_p * e^{-Ls}}{\alpha_1 s^3 + \alpha_2 s^2 + \alpha_3 s + \alpha_4} \quad (43)$$

Substitute $s = j\omega$ in (43) and separate into real and imaginary parts. By equating real and imaginary parts to zero, we can obtain K_p and K_i equations as like in (40) and (41). The denominator polynomial of (42) can be expressed as Kharitonov polynomials using (2) to (5). Using (6), we can obtain eight sets of equations. As necessary terms of numerator and denominator of each equation are substituted in (40) and (41), we can obtain K_p and K_i equations. By drawing the SBL for various values of ω, the stabilising values of K_p and K_i are obtained from the region where maximum loci are intersected.

6.2 KT for finding PI parameters for FC with time-delay

Consider a fuel cell plant $G_{FC}(s)$ with a time-delay (L). The open loop transfer function of FC by considering (23) is given as

$$G_{FC}(s) = \frac{K_p * e^{-Ls}}{\beta_1 s^4 + \beta_2 s^3 + \beta_3 s^2 + \beta_4 + 1} \quad (44)$$

where $\beta_{1=}T_P T_{FC} T_{IN} T_{IC}$, $\beta_2 = T_P T_{FC} T_{IN} + T_{FC} T_{IN} T_{IC} + T_{IN} T_{IC} T_P + T_{IC} T_P T_{FC}$, $\beta_3 = T_P T_{FC} + T_{FC} T_{IN} + T_{IN} T_{IC} + T_{IC} T_P + T_P T_{IN} + T_{FC} T_{IC}$, $\beta_4 = T_P + T_{FC} + T_{IN} + T_{IC}$

The closed loop characteristics (10) with PI controller of the form (8) is given by

$$\Delta(s)$$
$$= 1 + \left(K_p + \frac{K_i}{s}\right)\left[\frac{K_p * e^{-Ls}}{\beta_1 s^4 + \beta_2 s^3 + \beta_3 s^2 + \beta_4 + 1}\right] \quad (45)$$

The procedure followed in Section 6.1 is used to obtain the stabilising values of K_p and K_i for FC.

6.3 Finding PI parameters for DG and FC without time-delay

Consider (42) and (44) without time-delay. Using (2) to (5), four Kharitonov polynomials are to be formed. Using (6), eight sets of equations can be framed. As necessary terms of numerator and denominator of each equation are substituted in (15) and (17), we can obtain K_p and K_i equations. By drawing SBL for these equations for various values of ω, the stable values of K_p and K_i are obtained from the region where the maximum loci are intersected.

7. Numerical Example

7.1 PI parameters for DG with time-delay

Considering the uncertainty of the plant, the parameters of DG are varied ±20% from the nominal value and is given as K_p= [40,60], T_G= [0.064, 0.096], T_T = [0.32,

0.48], T_P = [8,12], R = [2.4, 3.6], L=1.0 s. (For eg, the nominal value of T_T =0.4 (from Table II) is varied ±20%. For +20%, T_T =0.48. For -20%, T_T=0.32)
Substituting the above values in (42), the DG transfer function, $G_{DG}(s)$, results:

$$G_{DG}(s) = \frac{[40, 60] * e^{-s}}{\begin{array}{c}[0.164, 0.533]s^3 + [3.1, 6.96]s^2 + \\ [8.38, 12.57]s \\ +[3.22, 5.16]\end{array}} \quad (46)$$

Now, the Kharitonov polynomials for the denominator of (46) are rewritten using (2)-(5) as
$Q_1(s) = 3.22 + 8.38s + 6.96s^2 + 0.553s^3$
$Q_2(s) = 3.22 + 12.57s + 6.96s^2 + 0.164s^3$

a

b
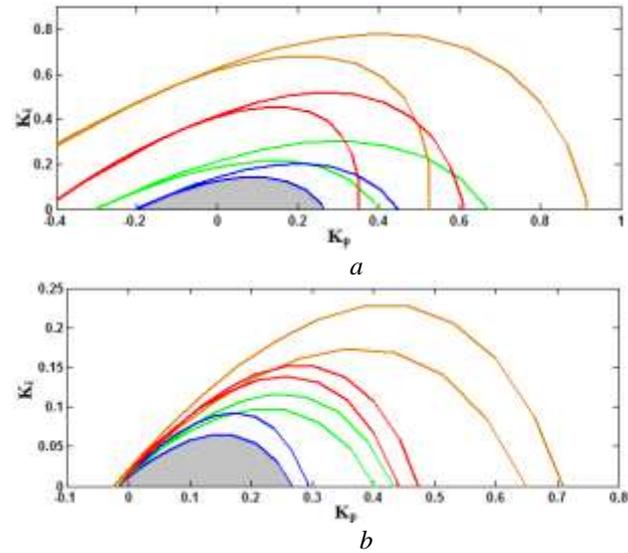
Fig.3 *Stability boundary locus*
a Diesel Generator locus with time-delay
b Fuel Cell locus with time-delay

$Q_3(s) = 5.16 + 8.38s + 3.1s^2 + 0.553s^3$
$Q_4(s) = 5.16 + 12.57s + 3.1s^2 + 0.164s^3 \quad (47)$
Using (6), the framed eight equations are defined as:

$$G_1(s) = \frac{40}{Q_1(s)}, G_2(s) = \frac{60}{Q_1(s)},$$

$$G_3(s) = \frac{40}{Q_2(s)}, \quad G_4(s) = \frac{60}{Q_2(s)},$$

$$G_5(s) = \frac{40}{Q_3(s)}, G_6(s) = \frac{60}{Q_3(s)},$$

$$G_7(s) = \frac{40}{Q_4(s)}, G_8(s) = \frac{60}{Q_4(s)}$$

$\quad (48)$

Substituting for Q₁(s) from (47) in (48) we get
$G_1(s) = 40/3.22 + 8.38s + 6.96s^2 + 0.553s^3 \quad (49)$

7

From (49) obtain the numerator real (N_{real}) and imaginary (N_{imag}) terms. For denominator obtain the real (D_{real}) and imaginary (D_{imag}) terms .We get

$$N_{imag} = 0; \quad N_{real} = 40; \quad \boldsymbol{D_{imag}} = -0.553 * \omega^2 + 8.38;$$
$$D_{real} = -6.94 * \omega^2 + 3.22 \tag{50}$$

Likewise, substitute each terms of (47) in (48) and separate the numerator and denominator terms of each equation of (48) into real and imaginary terms. Now, substituting the necessary terms of numerator and denominator of each equation of (48) in (40) and (41), we can obtain eight sets of K_p and K_i equations. By drawing the SBL for various values of ω, the stabilising values of K_p and K_i are obtained. Fig. 3a shows the SBL drawn for the DG. The dark region in the figure shows the stable values of $K_p \in$ [-0.2 to 0.27] and $K_i \in$ [0 to 0.145].The dark region contains all the stable of the PI controller parameters. In this work, maximum values of K_p and K_i are selected from the dark region.

7.2 Finding PI parameters for FC with time-delay

Considering the uncertainty of the plant, the parameters of FC are varied ±20% from the nominal value, and the values are

K_p= [40,60], T_P=[8,12], T_{FC}=[0.208, 0.312], T_{IN} =[0.032, 0.048], T_{IC} =[0.0032, 0.0048], L=1 s

Substituting the above values in (44), the FC transfer function, $G_{FC}(s)$, results:

$$G_{FC}(s)$$
$$= \frac{[40, 60] * e^{-s}}{[0.00017, 0.000862]s^4 + [0.059, 0.2]s^3 + [1.95, 4.52]s^2 + [8.24, 12.36]s + 1} \tag{51}$$

Now, the Kharitonov polynomials for the denominator of (51), are written using (2)-(5) as

$$Q_1(s) = 1 + 8.24s + 4.52s^2 + 0.2s^3 + 0.00017s^4$$
$$Q_2(s) = 1 + 12.36s + 4.52s^2 + 0.059s^3 + 0.00017s^4$$
$$Q_3(s) = 1 + 8.24s + 1.95s^2 + 0.2s^3 + 0.000862s^4$$
$$Q_4(s) = 1 + 12.36s + 1.95s^2 + 0.059s^3$$
$$+ 0.000862s^4 \tag{52}$$

Using (52), the framed eight equations are written as in (48). The remaining procedure is same as in section 7.1. Fig. 3b shows the SBL for FC. The dark area where maximum loci covered is the stability region. It is found that stable values of $K_p \in$ [-0.02 to 0.27] and $K_i \in$ [0 to 0.065].

7.3 Finding PI parameters for DG and FC systems without time-delay

The procedure given in section 6.3 is followed to find the PI parameters for DG and FC system without time-delay. Substitute each term of (47) in (48) and separate the numerator and denominator terms of each equation of (48) into imaginary and real terms. Now, substitute in in (15) and

(17), we can obtain eight sets of K_p and K_i equations. By drawing the SBL for various values of ω, the stabilising values of K_p and K_i are obtained.

The following figures 4a and 4b show the SBL for DG and FC systems without time-delay. The PI parameters are found using KT. It is found that stable values of $K_p \in$ [0.1 to 0.6] and $K_i \in$ [0.3 to 0.6] for DG. For FC, stable values of K_p ε [0.1 to 1.3] and K_i ε [0.2 to 1.15].

8. Simulation results

In this section, the simulation results for the stable values of K_p and K_i obtained using KT, considering DG and FC with and without time-delay is presented. The μG system is simulated for the interval system parameters in which they are varied ±20% from the nominal value. The variation of wind speed [36] is shown in Fig. 4a(i). For the given wind speed (V_w), the mechanical power output (P_w) of WTG is calculated using (20), which is displayed in Fig.


a

b
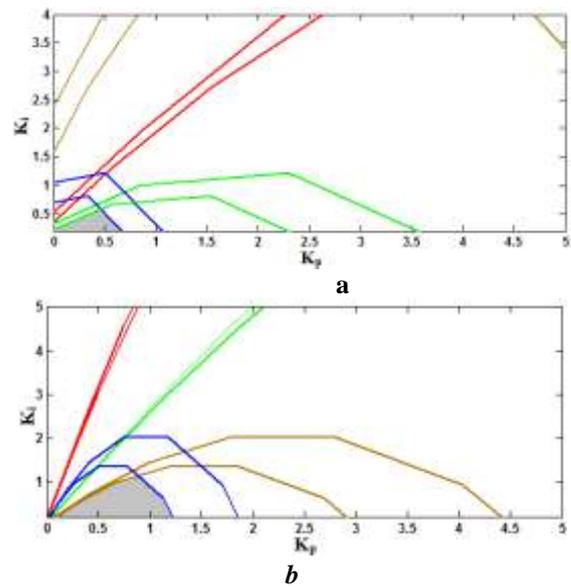
Fig.4 Stability boundary locus
  a Diesel Generator locus without time-delay
  b Fuel Cell locus without time-delay

5a(ii).

The total load demand (P_s^*) is 1.0 pu and the time-delay (L) considered is 1.0 s. In [27], a time-delay of 3.0 s is assumed for the LFC of the single area power system. Fig. 5b shows the DG power output. Whenever wind power fluctuates, DG generates the power in order to compensate for the frequency deviations. Initially, DG raises its generation up to 0.48 pu, and 0.38 pu for the PI controllers found by KT for the system with and without time-delay at 5.0 s and then follows with the rise and fall of WTG power output. The DG considered without time-delay responds immediately. At the same time, the DG takes 0.4 s to respond when the time-delay is considered.

Fig. 5c shows the FC power output. Whenever WTG wer output reduces, FC raises its power output to meet the demand and maintains the frequency deviation within the limit. FC raises its generation up to 0.52 pu and 1.3 pu for the PI controllers found by KT for the system with time-

delay and without time-delay and then follows with WTG power output.

Fig. 5d shows the BESS power output. BESS is capable of supplying instant power for the power deficit. When the WTG power output is more, BESS stores and releases the power when power deficit occurs. To meet the load demand, BESS raises its power output up to 0.58 pu and 0.4 pu for with and without time-delay systems for the PI controllers found by KT. The positive sign indicates the charging of BESS.

Fig. 6a shows the frequency deviations of the μG. From the fig.6a, it is evident that the system with time-delay has an impact on the system response. The peak overshoot of the frequency deviations for the system with and without time-delay is -0.43 Hz and -0.27 Hz. Also, the system takes 6 s to restore to its original state when the time-delay is considered. Whereas PI controllers tuned using ZN method with time-delay has peak overshoot of -0.62 Hz and the system settles after 20 s.

The robustness of the PI controller found using KT is shown for the frequency deviation for the load of 0.9 pu and 1.1 pu in fig. 6b and 6c. In fig. 6b, as the load is decreased from 1.0 pu to 0.9 pu, the peak overshoot of the frequency deviation is reduced to -0.39 Hz and the system takes 7 s to settle for the system with time-delay. In fig.6c, when the load is increased from 1.0 pu to 1.1 pu, the peak overshoot is raised to -0.47 Hz and the system takes 7 s to settle for the system with time-delay. The simulation results show that the frequency deviations are within the prescribed limit for the PI controllers found by KT.

Fig. 6 *Frequency responses for different system loads*

a Frequency deviation for the system load of 1.0 pu
b Frequency deviation for the system load of 0.9 pu
c Frequency deviation for the system load of 1.1 pu
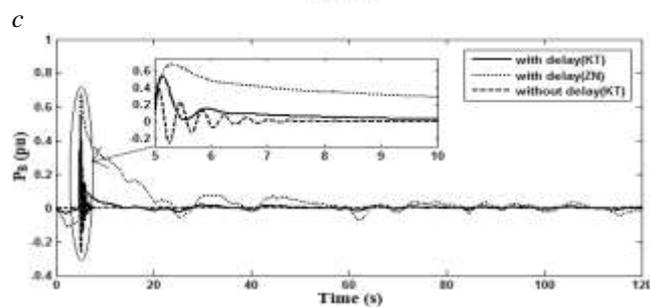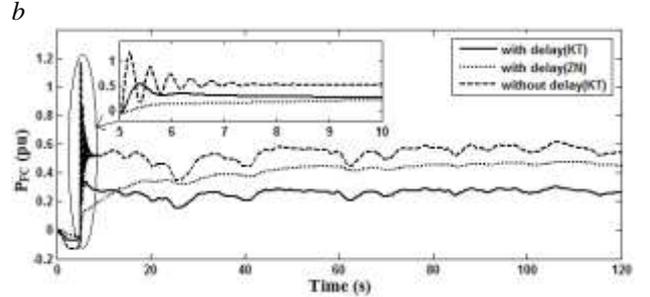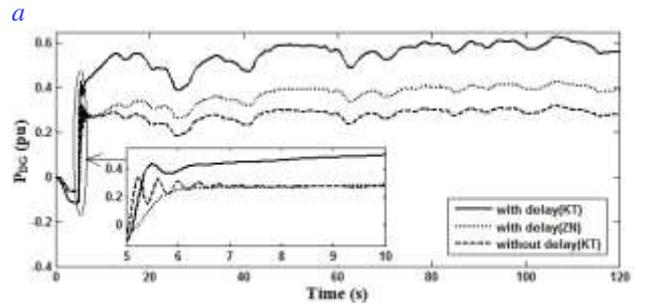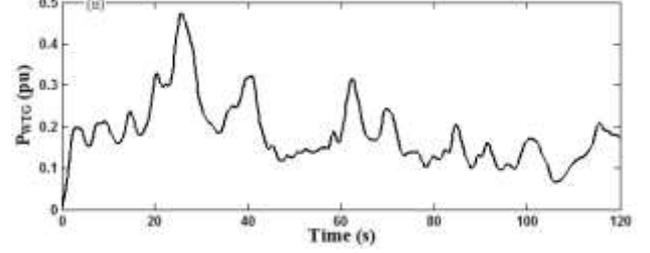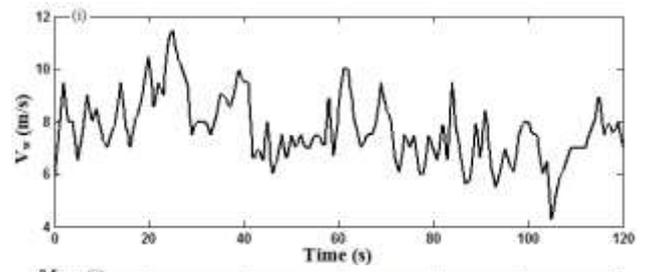
Fig. 5 Responses of the sources
a (i) Wind velocity (ii) WTG output power
*b* DG output power
c FC output power
d BESS output power

In fig. 6b and 6c, the peak overshoot is -0.56 Hz for the load of 0.9 pu and -0.7 Hz for the load of 1.1 pu for the ZN tuned PI controllers. The peak overshoot of the frequency deviation is more for ZN tuned PI controllers when compared with KT based PI controllers.

Fig. 7a shows the frequency deviation for the time-delay of 0.1 s. From the response it can be observed that the peak overshoot for a time-delay of 0.1s is -0.41Hz which is less when compared with the peak overshoot for the time-delay of 1 s. Fig. 7b shows the frequency deviation for the time-delay of 3 s. The peak overshoot of the frequency

deviation is -0.48 Hz and the system takes 8.0 s to settle which is more when compared to the time-delay of 1 s. As time-delay increases, the time taken for the frequency stabilization also increases.

9. Conclusion

Existing scientific literature in the area of LFC design has not taken communication time-delay effects or parameter uncertainties of the μG sources into consideration. The major contribution of this paper is it has proposed and demonstrated the suitability of a viable simple method using KT for calculating the PI controller parameters of μG sources with persisting communication
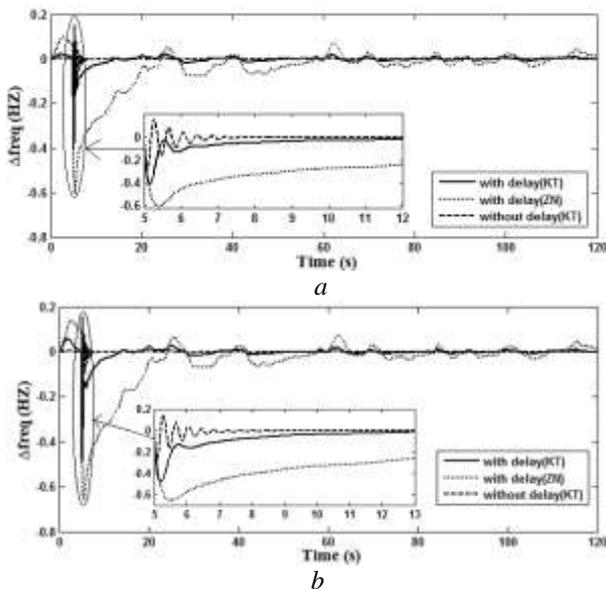
Fig. 7 Frequency responses for different time-delays

a Frequency deviation of the system with 0.1 s time-delay
b Frequency deviation of the system with 3.0 s time-delay

time-delays and system parametric uncertainties. Increase in time delays often has a deteriorating effect on the frequency stability of the system. With the adoption of KT based model, it would be easier to overcome the instabilities introduced because of communication time-delay. Robustness check is done for a load change of ±10% from the nominal value; the system frequency is within the tolerance limits for the PI controllers found using KT. In addition, the frequency deviations of the system for increase and decrease in communication time-delays have been examined with the obtained controller parameters. The frequency deviation is maintained well within the stable limits by the PI controllers so found by KT.

10 References

[1] Marzband,M., Moghaddam, M.M., Akorede, M.F., Khomeyarni, G.: 'Adaptive load shedding scheme for frequency stability enhancement in microgrids,' Electr. Power Syst. Res., 2016, 140, pp. 78–86.

[2] Aghamohammadi, M.R., Abdolahinia, H.: 'A new approach for optimal sizing of battery energy storage system for primary frequency control of islanded Microgrid', Int. J. Electr. Power Energy Syst., 2014, 54, pp. 325-333.

[3] Ray, P.K., Mohanty, S.R., Kishor, N.: 'Proportional–integral controller based small-signal analysis of hybrid distributed generation systems', Ener. Convers. manag , 2011, 52 pp. 1943–1954.

[4] Jafari, H., Mahmadi, M., Rastegar, H.: 'Frequency Control Of Micro-Grid in Autonomous Mode Using Model Predictive control', IEEE Iran Sect. Iran. Conf. Smart Grid, 2012, pp.1-6.

[5] Şerban, I., Marinescu, C.: 'Aggregate load-frequency control of a wind-hydro autonomous microgrid', Renew. Energy, 2011, 36, (12), pp. 3345–3354.

[6] Li, J., Yang, Q., Yao, P., et al.: 'A Novel use of the Hybrid Energy Storage System for Primary Frequency Control in a Microgrid', Energy Procedia, 2016, 103, pp. 82–87.

[7] Vidyanandan, K.V., Senroy, N.: 'Frequency regulation in a wind–diesel powered microgrid using flywheels and Fuel Cell', IET Gener. Transm. Distrib., 2016, 10, (3), pp. 780–788.

[8] Nayeripour, M., Hoseintabar, M., Niknam, T.: 'Frequency deviation control by coordination control of FC and double-layer capacitor in an autonomous hybrid renewable energy power generation system', Renew. Energy , 2011, 36, (6), pp. 1741-46.

[9] Mishra, S., Sharma, R., Sharma, D.: 'Coordinated active power control of wind, Solar and Diesel Generator in a microgrid', IFAC-Papersonline, 2015, 48, (30), pp.7-12.

[10] Mishra, S., Mallesham, G., Jha, A.N.: 'Design of controller and communication for frequency regulation of a smart microgrid', IET Renew. Power Gener., 2012, 6, (4), pp. 248-258.

[11] Khooban, M.H., Niknam, T., Blaabjerg, F., et al.: 'A new load frequency control strategy for micro-grids with considering electrical vehicles', Electr. Power Syst. Res., 2017, 143, pp. 585–598.

[12] Fazeli, M., Asher, G.M., Klumpner, C., et al.: 'Novel Integration of Wind Generator-Energy Storage Systems Within Microgrids', IEEE Trans. Smart Grid, 2012, 3, (2), pp. 728-737.

[13] Ahumada, C., Cardenas, R., Saez, D., et al.: 'Secondary Control Strategies for Frequency Restoration in Islanded Microgrids With Consideration of Communication Delays', IEEE Trans. Smart Grid, 2016, 7, (3), pp. 1430–1441.

[14] Chong, W.: 'Frequency Stabilization Design for Interconnected Microgrid based on T-S Fuzzy Model with Multiple Time Delays', 2016, pp. 1-6.

[15] Liu,S., Wang,X., Liu,P.X.: 'Impact of Communication Delays on Secondary Frequency Control in an Islanded Microgrid', IEEE Trans. Indus. Electr,2015,62,(4),pp.2021-2031.

[16] Vilanova, R., Pedret, C., Barbu, M.: 'PI-IMC Control for Frequency Deviation Control in Islanded Micro Grid', IEEE Int. Conf. Syst. Theo. Cont. Comp,2017, pp.777-784.

[17] Khooban, M.H.: 'Secondary Load Frequency Control of Time-Delay Stand-Alone Microgrids With Electric Vehicles', IEEE Trans. Indus. Electr, 2018, 65, (9), pp.7416-7422.

[18] Macana,C.A., Nava,E.M., Quijano,N.: 'Time-Delay Effect on Load Frequency Control for Microgrids', IEEE Int. conf. networking, sensing and control,2013, pp. 544-549.

[19] Saxena, S., Hote, Y.V.: 'Decentralized PID load frequency control for perturbed multi-area power systems', Int. J. Electr. Power Energy Syst., 2016, 81, pp. 405–415.

[20] Dehkordi,N,M.,Sadati,N.,Hamzeh,M., 'Distributed Robust Finite-Time Secondary Voltage and Frequency Control of Islanded Microgrids', IEEE Trans. Power Syst, 2017, 32, (5), pp.3648-3659.

[21] Vachirasricirikul, S., Ngamroo,I.: 'Robust controller design of Microturbine and Electrolyzer for Frequency Stabilization in a Microgrid System with Plug-in Hybrid Electric Vehicles', Int. J. Electr. Power Energy Syst., 2012, 43, (1), pp. 804-811.

[22] Supriyadi,C., Nandar,A.: 'Robust PI control of smart controllable load for frequency stabilization of microgrid power system', Renew. Energy, 2013, 56, pp. 16-23.

[23] Khodadadi,A, Divshali,P.H,Nazari, M.H,et al.: 'Small-signal stability improvement of an islanded microgrid with electronically-interfaced distributed energy resources in the presence of parametric uncertainties', Elect. Power Syst. Resear, 2018,(160),pp. 151–162

[24] Padhan, D.G., Majhi, S.: 'A new control scheme for PID load frequency controller of single-area and multi-area power systems' ISA Trans., 2013, 52, (2), pp. 242–251.

[25] Olivares, D., Sani,A., Etemadi,A., et al.: 'Trends in microgrid control', IEEE Trans. Smart Grid, 2014, 5, (4), pp. 1905–1919.

[26] Khalil, A., Rajab, Z., Alfergani, A., et al.: 'The impact of the time delay on the load frequency control system in microgrid with plug-in-electric vehicles', Sustain. Cities Soc., 2017, 35, pp. 365–377.

[27] Ojaghi, P., Rahmani, M.: 'LMI-Based Robust Predictive Load Frequency Control for Power Systems With Communication Delays', IEEE Trans. Power Syst., 2017, 32, (5), pp. 4091–4100.

[28] Mary, T.J., Rangarajan, P.: 'Delay-dependent Stability Analysis of Microgrid with Constant and Time-varying Communication Delays', Electr. Power Comp. Syst., 2016, 44, (13), pp. 1441–1452.

[29] Gunduz, H., Sonmez, S., Ayasun,S.: 'Comprehensive gain and phase margins based stability analysis of micro-grid frequency control system with constant communication time delays', IET Gener. Transm. Distrib., 2017, 11, (3), pp. 719–729.

[30] Jiang, L., Yao, W., Wu, Q.H., et al.: 'Delay-dependent stability for load frequency control with constant and time-varying delays,' IEEE Trans. Power Syst., 2012, 27, (2), pp. 932–941.

[31] Shankar,G., Mukherjee.V: 'Load frequency control of an autonomous hybrid power system by quasi-oppositional harmony search algorithm', Electr. Power Ener. Syst., 2016, 78, pp. 715–734.

[32] Mallesham, G., Mishra, S., Jha, A.N.: Ziegler-Nichols based Controller Parameters Tuning for Load Frequency Control in a Microgrid, Int. conf. Energy, Autom. signal(ICEAS), 2011, pp.1-8.

[33] Matusu.R.,Prokop.: Computation of Robustly Stabilizing PID Controllers for Interval Systems, Springer Plus., 2016, 5, (6), pp.1-16.

[34] Bevrani, H., Habibi, F., Babahajyani,P., et al.: 'Intelligent Frequency Control in an AC MG: Online PSO-based fuzzy tuning approach', IEEE Trans. Smart Grid. 2012, 3, (4), pp. 1935–1944.

[35] Deniz,N.F., Tan, N. : A model identification method for tuning of PID controller in a smith predictor structure, IFAC-Papersonline, 2016, 49, (10), pp.13-18.

[36] Available at http:// renknownet2.iwes.fraunhofer.de/pages_en/objektdatenbank_en.htm